Construction of Symmetric Framelets and their Applications

Myungjin Choi

Division of Applied Mathematics,
Satellite Technology Research Center,
Korea Advanced Institute of Science and Technology

April 21, 2006

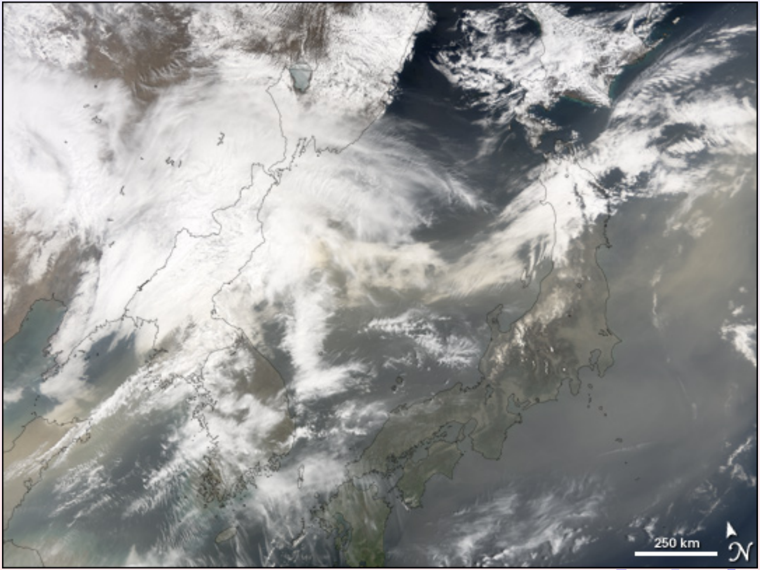
250 km
N

Outline

1. General framelets
   - Preliminaries
   - Symmetric framelets
2. Filter Design
   - Symmetric framelets with two generators
   - Symmetric framelets with three generators
3. Applications
   - Image Denoising
   - Image Fusion

Outline

1. General framelets
   - Preliminaries
   - Symmetric framelets
2. Filter Design
   - Symmetric framelets with two generators
   - Symmetric framelets with three generators
3. Applications
   - Image Denoising
   - Image Fusion

Outline

1. General framelets
   - Preliminaries
   - Symmetric framelets
2. Filter Design
   - Symmetric framelets with two generators
   - Symmetric framelets with three generators
3. Applications
   - Image Denoising
   - Image Fusion

Outline

Preliminaries

Suppose a real-valued function $\phi \in L^2(\mathbb{R})$ satisfies the following conditions:

(a) $\hat{\phi}(\omega) = m_0(\omega/2)\hat{\phi}(\omega/2)$, where m_0 is an essentially bounded 2π-periodic function; and

(b) $\lim_{\omega \to 0} \hat{\phi}(\omega) = 1$; $\quad \Rightarrow \quad \hat{\phi}(\omega) = \prod_{j=1}^{\infty} m_0(\omega/2^j)$,

then the function ϕ is called refinable or scaling, m_0 is called a symbol of ϕ, and the relation in item (a) is called a refinement equation.

Preliminaries

Every refinable function generates multiresolution analysis (MRA) of the space $\phi \in L^2(\mathbb{R})$, i.e., a nested sequence

$$\cdots \subset V^{-1} \subset V^0 \subset V^1 \subset \cdots \subset V^j \subset \cdots$$

of closed linear subspaces of $\phi \in L^2(\mathbb{R})$ such that:

(a) $\bigcap_{j\in\mathbb{Z}} V^j = \varnothing$;

(b) $\overline{\bigcup_{j\in\mathbb{Z}} V^j} = L^2(\mathbb{R})$; and

(c) $f(x) \in V^j \Leftrightarrow f(2x) \in V^{j+1}$.

Preliminaries

If we denote by W^j the orthogonal complement of the space V^j in V^{j+1}, then the function ψ (which is called a wavelet), defined by the relation

$$\hat{\psi}(\omega) := m_\psi(\omega/2)\hat{\phi}(\omega/2)$$

where $m_\psi(\omega) = \overline{e^{i\omega} m_\phi(\omega + \pi)}$, generates an orthonormal basis $\{\psi(x-k)\}_{k\in\mathbb{Z}}$ of the space W^0. Thus, the system

$$\{2^{j/2}\psi(2^j x - k)\}_{j,k\in\mathbb{Z}}$$

constitutes an orthonormal basis of the space $L^2(\mathbb{R})$.

Preliminaries

The problem of finding orthonormal wavelet bases, generated by a scaling function, can be reduced to solving the matrix equation

$$\mathbf{M}(\omega)\mathbf{M}^*(\omega) = I,$$

where

$$\mathbf{M}(\omega) = \begin{pmatrix} m_0(\omega) & m_1(\omega) \\ m_0(\omega+\pi) & m_1(\omega+\pi) \end{pmatrix},$$

$m_0(\omega)$, $m_1(\omega)$ are essentially bounded functions, and $m_0(-\omega) = \overline{m_0(\omega)}$.

Preliminaries

A frame in a Hilbert space *H* is a family of its elements $\{f_k\}_{k\in\mathbb{Z}}$ such that, for any $f \in$ *H*,

$$A\|f\|^2 \leq \sum_{k\in\mathbb{Z}} |\langle f, f_k\rangle|^2 \leq B\|f\|^2,$$

where optimal A and B are called frame constants. If $A = B$, the frame is called a tight frame.
In the case when a tight frame has unit frame constants (e.g., if it is an orthonormal basis) for any function $f \in L^2(\mathbb{R})$, the expansion

$$f = \sum_{n\in\mathbb{Z}} \langle f_n, f\rangle f_n$$

is valid.

Preliminaries

Let ϕ be a refinable function with m_0, $\hat{\psi}^k(\omega) = m_k(\omega/2)\hat{\phi}(\omega/2)$, where each symbol m_k is a 2π-periodic and essentially bounded function for $k = 1, 2, \dots, n$.
It is well-known (A.Ron and Z.Shen, 1997) that for constructing tight frames with the property

$$M(\omega)M^*(\omega) = I \tag{1}$$

the matrix

$$M(\omega) = \begin{pmatrix} m_0(\omega) & m_1(\omega) & \cdots & m_n(\omega) \\ m_0(\omega+\pi) & m_1(\omega+\pi) & \cdots & m_n(\omega+\pi) \end{pmatrix}$$

plays an important role.

Preliminaries

Theorem 1

If (1) holds, then the functions $\{\psi^1, \psi^2, \ldots, \psi^n\}$ generate a tight frame of $L^2(\mathbb{R})$.

Theorem 2 [Chui(2000) and Petukhov (2001)]

Equation $M(\omega)M^*(\omega) = I$ has a solution if and only if

$$|m_0(\omega)|^2 + |m_0(\omega+\pi)|^2 \leqslant 1(a.e.). \tag{2}$$

Preliminaries

Theorem 1

If (1) holds, then the functions $\{\psi^1, \psi^2, \ldots, \psi^n\}$ generate a tight frame of $L^2(\mathbb{R})$.

Theorem 2 [Chui(2000) and Petukhov (2001)]

Equation $M(\omega)M^*(\omega) = I$ has a solution if and only if

$$|m_0(\omega)|^2 + |m_0(\omega+\pi)|^2 \leqslant 1(a.e.). \quad (2)$$

Preliminaries

$$\tilde{M}(\omega) := M_\psi(\omega) M_\psi^*(\omega) = \begin{pmatrix} 1 - |m_0(\omega)|^2 & -m_0(\omega)\overline{m_0(\omega+\pi)} \\ -\overline{m_0(\omega)}m_0(\omega+\pi) & 1 - |m_0(\omega+\pi)|^2 \end{pmatrix}$$

where

$$M_\psi(\omega) = \begin{pmatrix} m_1(\omega) & m_2(\omega) & \cdots & m_n(\omega) \\ m_1(\omega+\pi) & m_2(\omega+\pi) & \cdots & m_n(\omega+\pi) \end{pmatrix}.$$

Let us introduce the diagonal matrix $\Lambda(\omega)$ with eigenvalues of the matrix $\tilde{M}(\omega)$ on the diagonal and the matrix $P(\omega)$ whose columns are the corresponding eigenvectors. Then

$$\Lambda(\omega) = \begin{pmatrix} 1 & 0 \\ 0 & 1 - |m_0(\omega)|^2 - |m_0(\omega+\pi)|^2 \end{pmatrix}.$$

Preliminaries

Theorem 3 [Petukhov (2001)]

Let a 2π-periodic function $m_0(\omega)$ satisfy (2). Then there exists a pair of 2π-periodic measurable functions m_1, m_2 which satisfy (1) for $n = 2$. Any solution of (1) can be represented in the form of the first row of the matrix

$$M_\psi(\omega) = P(\omega)D(\omega)Q(\omega),$$

where $D(\omega)$ is a diagonal matrix, $D(\omega)\overline{D(\omega)} = \Lambda(\omega)$, and $Q(\omega)$ is an arbitrary unitary (a.e.) matrix with π-periodic measurable components.

Preliminaries

Theorem 4 [Chui(2000) and Petukhov (2001)]

Let a trigonometric polynomial $m_0(\omega)$ of degree n satisfy (2). Then there exists a pair of trigonometric polynomials m_1, m_2 of degree at most n that satisfies (1).

Theorem 5 [Chui(2000)]

For any refinable function ϕ with a polynomial symbol m_0 there are three (anti)symmetric functions m_1, m_2, m_3, providing a solution to (1).

Preliminaries

Theorem 4 [Chui(2000) and Petukhov (2001)]

Let a trigonometric polynomial $m_0(\omega)$ of degree n satisfy (2). Then there exists a pair of trigonometric polynomials m_1, m_2 of degree at most n that satisfies (1).

Theorem 5 [Chui(2000)]

For any refinable function ϕ with a polynomial symbol m_0 there are three (anti)symmetric functions m_1, m_2, m_3, providing a solution to (1).

Outline

Symmetric condition

In what follows, the $H_k(z)$ are specified by the z-transform of the symbols $m_k(\omega)$, i.e., $H_k(e^{i\omega}) := m_k(\omega)$.

Theorem 6 [Petukhov(2003)]

Let $H_0(z)$ be a symmetric Laurent polynomial of degree n, satisfying (2). Then two (anti)symmetric solutions to (1) exist if and only if all roots of the Laurent polynomial

$$H(z) := 1 - H_0(z)H_0(1/z) - H_0(-z)H_0(-1/z)$$

have even multiplicity.

Corollary 1

Corollary 1

For the refinable functions B_n two (anti)symmetric solutions exist for $n = 1, 2, 3, 7$ and do not exist for other n.

Corollary 2

An interpolatory symbol H_0 admits (anti)symmetric solutions to (1) if and only if $H_0(z) = (z^{1-2N} + 2 + z^{2N-1})/4$.

Corollary 1

Corollary 1

For the refinable functions B_n two (anti)symmetric solutions exist for $n = 1, 2, 3, 7$ and do not exist for other n.

Corollary 2

An interpolatory symbol H_0 admits (anti)symmetric solutions to (1) if and only if $H_0(z) = (z^{1-2N} + 2 + z^{2N-1})/4$.

Outline

Symmetric framelets with two generators [Selesnick (2004)]

$$H_k(z) := \sum_n h_k(n) z^{-n}.$$

Let h_0,h_1,h_2 be three filters where the lowpass filter $h_0(n)$ is symmetric, the filters $h_1(n)$ and $h_2(n)$ are each either symmetric or antisymmetric, and $h_2(n)$ is a time-reversed version of $h_1(n)$. That is,

$$h_0(n) = h_0(N-1-n), h_2(n) = h_1(N-1-n). \tag{3}$$

Symmetric framelets with two generators

Lemma 1 [Selesnick (2004)]

The filters $\{h_0, h_1, h_2\}$ with symmetries (3) satisfy the paraunitary condition if their polyphase components are given by

$$H_{0e}(z) = z^{-N/2}\sqrt{2}A(z)B(1/z),$$
$$H_{1e}(z) = A^2(z),$$
$$H_{1o}(z) = -B^2(z),$$

where $A(z)$ and $B(z)$ satisfy $A(z)A(1/z) + B(z)B(1/z) = 1$.

Symmetric framelets with two generators

Our construction of $h_0(n)$ will be based on the maximally-flat lowpass even-length FIR filter, which has the following transfer function:

$$F^{M,L}(z) =$$

$$\frac{1}{2}(1+z^{-1})\left(\frac{z+2+z^{-1}}{4}\right)^M \sum_{n=0}^{L} \binom{M+n-0.5}{n} \left(\frac{-z+2-z^{-1}}{4}\right)^n .$$

If $\sqrt{2}F^{(M,L)}(z)$ is used as a scaling filter $H_0(z)$ then each wavelet will have at least $L+1$ vanishing moments. This is because $1-F^{(M,L)}(z)F^{(M,L)}(1/z)$ has $(1-z)^{2L+2}$ as a factor.

Symmetric framelets with two generators

Unfortunately, setting $H_0(z) := F^{(M,L)}(z)$ gives an $H_0(z)$ that does not satisfy the condition of Thm.6. That is, $1 - 2H_{0e}(z)H_{0e}(1/z)$ will not have roots of even degree.

However, by using a linear combination of various $F^{(M,L)}(z)$, we can obtain a filter $H_0(z)$ that does satisfy the condition of Thm.6. For example, if we set

$$H_0(z) = z^{-4}\sqrt{2}(\alpha F^{(2,1)}(z) + (1-\alpha)F^{(3,1)}(z)),$$

then for special values of α, $H_0(z)$ satisfy the condition of Thm.6.

Symmetric framelets with two generators

$U^2(z) = 1 - H_{0e}(z)H_{0e}(1/z)$,
where $U(z) = H_{1e}(z)H_{1e}(1/z) - H_{1o}(z)H_{1o}(1/z)$.

$$
\begin{aligned}
U(z) =& A^2(z)A^2(1/z) - B^2(z)B^2(1/z) \\
=& [A(z)A(1/z) + B(z)B(1/z)][A(z)A(1/z) - B(z)B(1/z)] \\
=& A(z)A(1/z) - B(z)B(1/z) \\
=& 2A(z)A(1/z) - 1 \\
=& 1 - 2B(z)B(1/z)
\end{aligned}
$$

so
$A(z)A(1/z) = 0.5 + 0.5U(z)$
and
$B(z)B(1/z) = 0.5 - 0.5U(z)$.

Plot the scaling function and wavelets

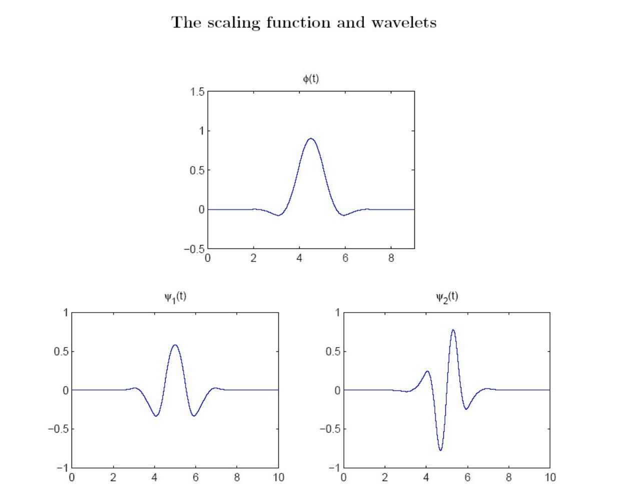

The fast framelet transform

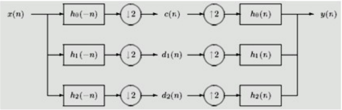

A 3-Channel Perfect Reconstruction Filter Bank

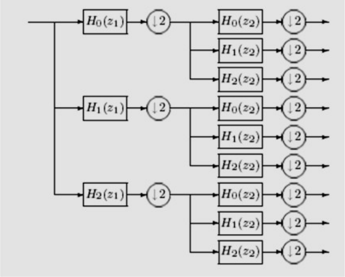

An Oversampled Filter Bank for 2-D Images

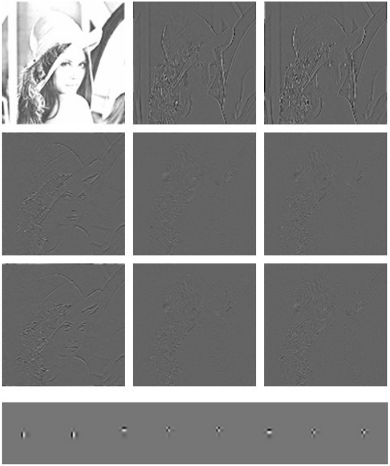

Outline

Symmetric framelets with three generators

$$\phi(t) = \sqrt{2}\sum_n h_0(n)\phi(2t-n)$$

$$\psi_i(t) = \sqrt{2}\sum_n h_i(n)\phi(2t-n), i = 1, 2, 3.$$

Define $\phi_k(t) := \phi(t-k)$, $\psi_{i,j,k}(t) := 2^{j/2}\psi_i(2^j t - k), i = 1, 2, 3.$

$$f(t) = \sum_{k=-\infty}^{\infty} c(k)\phi_k(t) + \sum_{i=1}^{3}\sum_{j=0}^{\infty}\sum_{k=-\infty}^{\infty} d_i(j,k)\psi_{i,j,k}(t),$$

$$c(k) = \int f(t)\phi_k(t)dt$$

$$d_i(j,k) = \int f(t)\psi_{i,j,k}(t)dt, i = 1, 2, 3.$$

The overcomplete filter bank

Take

$$\psi_3(t) = \psi_2(t - 0.5)$$

or equivalently

$$h_3(n) = h_2(n - 1).$$

Implementation of discrete transform uses the filter bank:

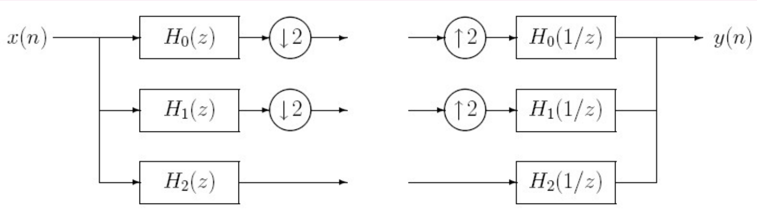

The sampling of the time-frequency plane

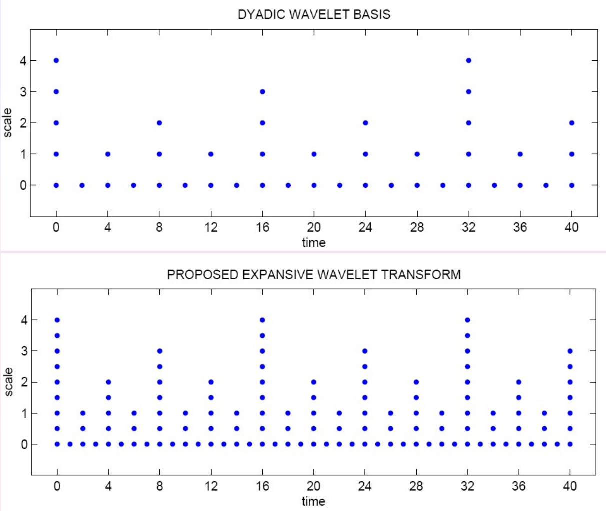

Perfect reconstruction conditions

$$
\begin{aligned}
Y(z) = {} & 0.5[H_0(z)X(z) + H_0(-z)X(-z)]H_0(1/z) \\
& + 0.5[H_1(z)X(z) + H_1(-z)X(-z)]H_1(1/z) + H_2(z)H_2(1/z)X(z).
\end{aligned}
$$

Rearranging,

$$
\begin{aligned}
Y(z) = {} & [0.5H_0(z)H_0(1/z) + 0.5H_1(z)H_1(1/z) + H_2(z)H_2(1/z)]X(z) \\
& + [0.5H_0(-z)H_0(1/z) + 0.5H_1(-z)H_1(1/z)]X(-z).
\end{aligned}
$$

Perfect reconstruction conditions

Therefore, for perfect reconstruction(PR), we need

$$H_0(z)H_0(1/z) + H_1(z)H_1(1/z) + 2H_2(z)H_2(1/z) = 2,$$
$$H_0(-z)H_0(1/z) + H_1(-z)H_1(1/z) = 0.$$

Define $H_1(z) = zH_0(-1/z)$.

Then, we have

$$\begin{aligned} H_1(-z)H_1(1/z) &= (-z)H_0(1/z)(1/z)H_0(-z) \\ &= -H_0(-z)H_0(1/z) \end{aligned}$$

$\Longrightarrow$ Second PR condition is satisfied!

Perfect reconstruction conditions

Now we have only to find $H_2(z)$ so as to satisfy the first PR condition.

$$\begin{aligned} 2H_2(z)H_2(1/z) &= 2 - H_0(z)H_0(1/z) - H_1(z)H_1(1/z) \\ &= A(z). \end{aligned}$$

In summary we have

$$\begin{aligned} H_1(z) &= zH_0(-1/z) \\ H_2(z) &= \sqrt{A(z)/2} \\ H_3(z) &= zH_2(z). \end{aligned}$$

Plot the scaling function and wavelets

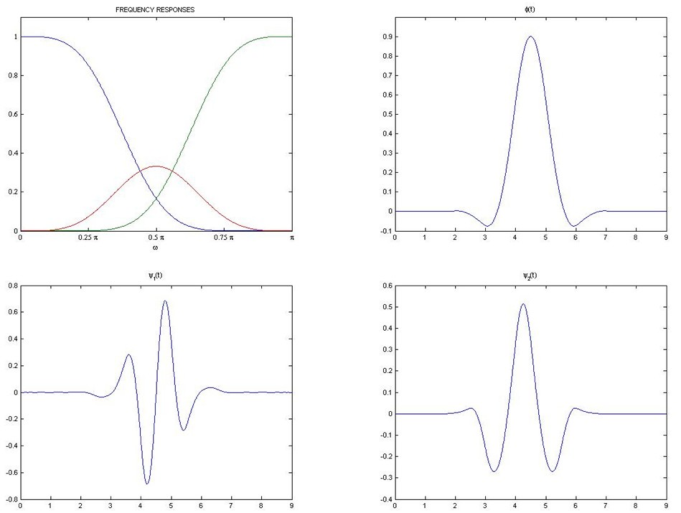

Outline

1D Signal Denoising

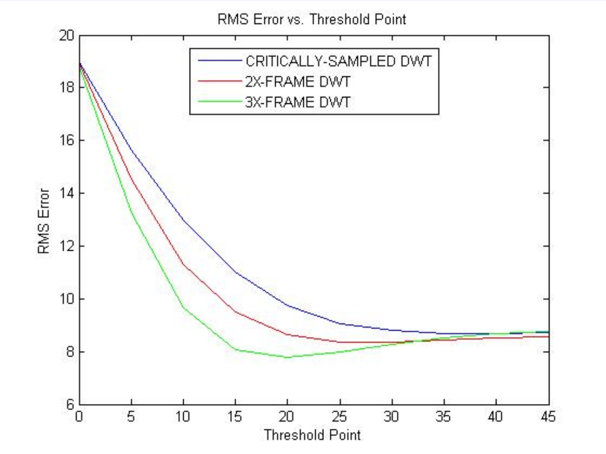

2D Image Denoising

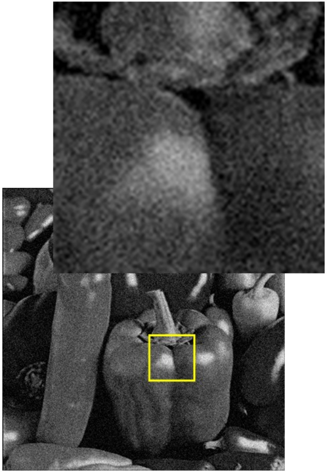

Noise image, σ=20, PSNR = 10.85 dB

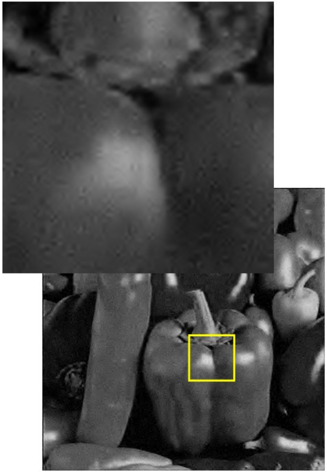

SW_Denoise image, PSNR = 12.72 dB

2D Image Denoising

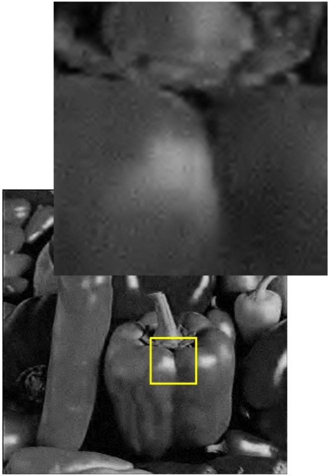

SW_Denoise image, PSNR = 12.72 dB

2W_Denoise image, PSNR = 13.52 dB

2D Image Denoising

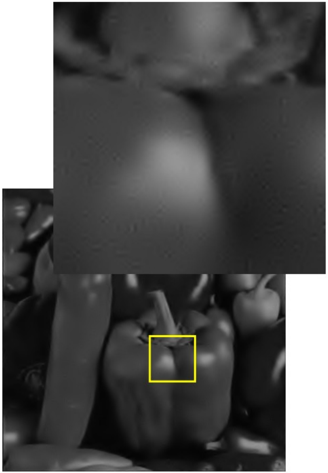

2W_Denoise image, PSNR = 13.52 dB

2W_Denoise image, PSNR = 16.78 dB

Outline

Why is image fusion important?

Technical limitations

- The incoming radiation energy to the sensor
- The data volume collected by the sensor
- On-board storage capacity
- Data transmission rates from platform to GS

QuickBird Characteristics	
Launch Date	October 18, 2001
Launch Vehicle	Boeing Delta II
Launch Location	Vandenberg Air Force Base, California
Orbit Altitude	450 km
Orbit Inclination	97.2 degree, sun-synchronous
Speed	7.1 km/second
Equator Crossing Time	10:30 a.m. (descending node)
Orbit Time	93.5 minutes
Revisit Time	1-3.5 days depending on latitude (30° off-nadir)
Swath Width	16.5 km at nadir
Metric Accuracy	23-meter horizontal (CE90%)
Digitization	11 bits
Resolution	Pan: 61 cm (nadir) to 72 cm (25° off-nadir) MS: 2.44 m (nadir) to 2.88 m (25° off-nadir)
Image Bands	Pan: 450 - 900 nm Blue: 450 - 520 nm Green: 520 - 600 nm Red: 630 - 690 nm Near IR: 760 - 900 nm

Why is image fusion important?

Technical limitations

- The incoming radiation energy to the sensor
- The data volume collected by the sensor
- On-board storage capacity
- Data transmission rates from platform to GS

QuickBird Characteristics	
Launch Date	October 18, 2001
Launch Vehicle	Boeing Delta II
Launch Location	Vandenberg Air Force Base, California
Orbit Altitude	450 km
Orbit Inclination	97.2 degree, sun-synchronous
Speed	7.1 km/second
Equator Crossing Time	10:30 a.m. (descending node)
Orbit Time	93.5 minutes
Revisit Time	1-3.5 days depending on latitude (30° off-nadir)
Swath Width	16.5 km at nadir
Metric Accuracy	23-meter horizontal (CE90%)
Digitization	11 bits
Resolution	Pan: 61 cm (nadir) to 72 cm (25° off-nadir) MS: 2.44 m (nadir) to 2.88 m (25° off-nadir)
Image Bands	Pan: 450 - 900 nm Blue: 450 - 520 nm Green: 520 - 600 nm Red: 630 - 690 nm Near IR: 760 - 900 nm

Why is image fusion important?

Technical limitations

- The incoming radiation energy to the sensor
- The data volume collected by the sensor
- On-board storage capacity
- Data transmission rates from platform to GS

QuickBird Characteristics	
Launch Date	October 18, 2001
Launch Vehicle	Boeing Delta II
Launch Location	Vandenberg Air Force Base, California
Orbit Altitude	450 km
Orbit Inclination	97.2 degree, sun-synchronous
Speed	7.1 km/second
Equator Crossing Time	10:30 a.m. (descending node)
Orbit Time	93.5 minutes
Revisit Time	1-3.5 days depending on latitude (30° off-nadir)
Swath Width	16.5 km at nadir
Metric Accuracy	23-meter horizontal (CE90%)
Digitization	11 bits
Resolution	Pan: 61 cm (nadir) to 72 cm (25° off-nadir) MS: 2.44 m (nadir) to 2.88 m (25° off-nadir)
Image Bands	Pan: 450 - 900 nm Blue: 450 - 520 nm Green: 520 - 600 nm Red: 630 - 690 nm Near IR: 760 - 900 nm

Why is image fusion important?

Technical limitations

- The incoming radiation energy to the sensor
- The data volume collected by the sensor
- On-board storage capacity
- Data transmission rates from platform to GS

QuickBird Characteristics	
Launch Date	October 18, 2001
Launch Vehicle	Boeing Delta II
Launch Location	Vandenberg Air Force Base, California
Orbit Altitude	450 km
Orbit Inclination	97.2 degree, sun-synchronous
Speed	7.1 km/second
Equator Crossing Time	10:30 a.m. (descending node)
Orbit Time	93.5 minutes
Revisit Time	1-3.5 days depending on latitude (30° off-nadir)
Swath Width	16.5 km at nadir
Metric Accuracy	23-meter horizontal (CE90%)
Digitization	11 bits
Resolution	Pan: 61 cm (nadir) to 72 cm (25° off-nadir) MS: 2.44 m (nadir) to 2.88 m (25° off-nadir)
Image Bands	Pan: 450 - 900 nm Blue: 450 - 520 nm Green: 520 - 600 nm Red: 630 - 690 nm Near IR: 760 - 900 nm

Why is image fusion important?

Effective fusion technique is a useful tool to

- Increase the ability of humans to interpret the image
- Improve the accuracy of the satellite image classification
- Give a visually beautiful color image
- Provide solution for GIS-based applications.

Why is image fusion important?

Effective fusion technique is a useful tool to

- Increase the ability of humans to interpret the image
- Improve the accuracy of the satellite image classification
- Give a visually beautiful color image
- Provide solution for GIS-based applications.

Why is image fusion important?

Effective fusion technique is a useful tool to

- Increase the ability of humans to interpret the image
- Improve the accuracy of the satellite image classification
- Give a visually beautiful color image
- Provide solution for GIS-based applications.

Why is image fusion important?

Effective fusion technique is a useful tool to

- Increase the ability of humans to interpret the image
- Improve the accuracy of the satellite image classification
- Give a visually beautiful color image
- Provide solution for GIS-based applications.

Standard method of image fusion

Two Points

1. how to extract the spatial information from panchromatic high-resolution image,
2. how to inject the extracted spatial information into the multispectral images.

Standard method of image fusion

Two Points

1. how to extract the spatial information from panchromatic high-resolution image,
2. how to inject the extracted spatial information into the multispectral images.

Two Steps

1. Decompose only the panchromatic image to n resolution levels,

$$PAN = \sum_{l=1}^{n} W_{P_l} + PAN_r.$$

2. Replace PAN_r by the R, G, and B bands of the multispectral images and perform the inverse wavelet transform.

$$F(R) = \sum_{l=1}^{n} W_{P_l} + R$$

$$F(G) = \sum_{l=1}^{n} W_{P_l} + G$$

$$F(B) = \sum_{l=1}^{n} W_{P_l} + B$$

Two Steps

1. Decompose only the panchromatic image to n resolution levels,

$$PAN = \sum_{l=1}^{n} W_{P_l} + PAN_r.$$

2. Replace PAN_r by the R, G, and B bands of the multispectral images and perform the inverse wavelet transform.

$$F(R) = \sum_{l=1}^{n} W_{P_l} + R$$

$$F(G) = \sum_{l=1}^{n} W_{P_l} + G$$

$$F(B) = \sum_{l=1}^{n} W_{P_l} + B$$

Test Set : IKONOS Imagery

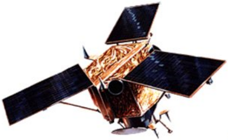

Launch Date	24 September 1999 Vandenberg Air Force Base, California
Operational Life	Over 8.5 Years
Orbit	98.1 degree, sun synchronous
Speed on Orbit	7.5 kilometers (4.7 miles) per second
Speed Over the Ground	6.8 kilometers (4.2 miles) per second
Number of Revolutions Around the Earth	14.7 every 24 hours
Orbit Time Around the Earth	98 minutes
Altitude	681 kilometers (423 miles)
Resolution	**Nadir:** 0.82 meters (2.7 feet) panchromatic 3.2 meters (10.5 feet) multispectral **26° Off-Nadir** 1.0 meter (3.3 feet) panchromatic 4.0 meters (13.1 feet) multispectral
Image Swath	11.3 kilometers (7.0 miles) at nadir 13.8 kilometers (8.6 miles at 26° off-nadir)
Equator Crossing Time	Nominally 10:30 a.m. solar time
Revisit Time	Approximately 3 days at 1-meter resolution, 40° latitude
Dynamic Range	11-bits per pixel
Image Bands	Panchromatic, blue, green, red, near infrared

Comparative Analysis

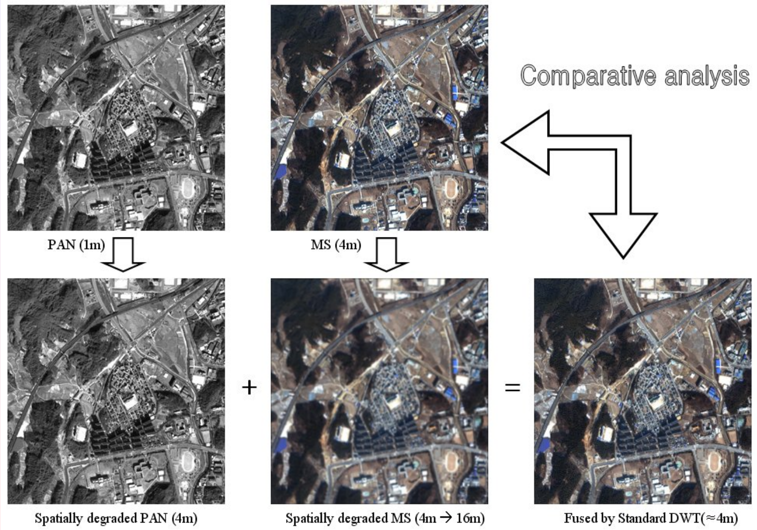

Quantitative Analysis

Spatial Quality : Zhou et al.

To evaluate the detailed spatial information, a procedure proposed by Zhou et al. is used. In this procedure, the PAN and fusion result are filtered by a Laplacian filter as follows:

$$\begin{vmatrix} -1 & -1 & -1 \\ -1 & 8 & -1 \\ -1 & -1 & -1 \end{vmatrix}$$

The high correlation coefficients between the fusion result and the PAN filtered image indicate that most of the spatial information of the PAN image was incorporated during the fusion process.

Quantitative Analysis

Spectral Quality : Q4

Let $Z_1 = a_1 + ib_1 + jc_1 + kd_1$ and $Z_2 = a_2 + ib_2 + jc_2 + kd_2$ denote the four-band original MS image and the fusion result, respectively, both expressed as quaternions.

$$Q_4 = \frac{|\sigma_{Z_1 Z_2}|}{\sigma_{Z_1} \cdot \sigma_{Z_2}} \cdot \frac{2\sigma_{Z_1} \cdot \sigma_{Z_2}}{\sigma_{Z_1}^2 + \sigma_{Z_2}^2} \cdot \frac{2|\bar{Z}_1| \cdot |\bar{Z}_2|}{|\bar{Z}_1|^2 + |\bar{Z}_2|^2}.$$

The first one is the modulus of the hypercomplex CC between Z_1 and Z_2 and is sensitive both to loss of correlation and to spectral distortion between the two MS datasets.
The second and third terms, respectively, measure contrast changes and mean bias on all bands simultaneously.

Quantitative Analysis

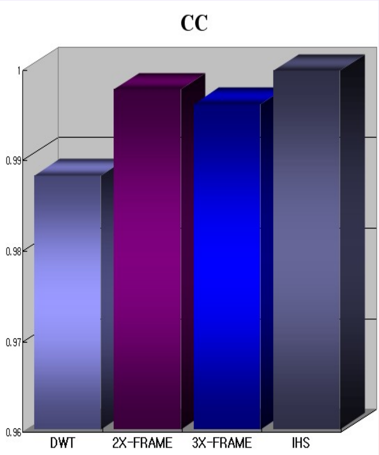

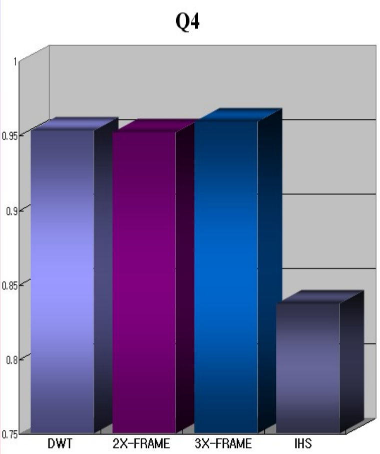

Visual Analysis

Original image

Visual Analysis

by Standard DWT

Visual Analysis

by IHS

Visual Analysis

by 2X-FRAME DWT

Visual Analysis

by 3X-FRAME DWT

Comparison

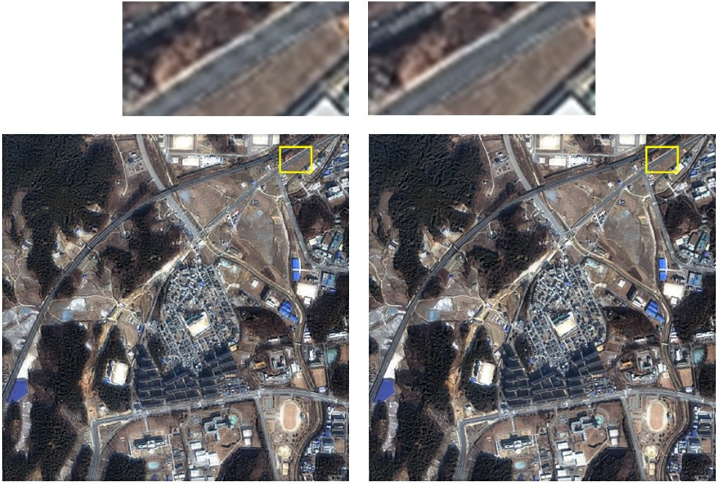

Fused by wavelets

Fused by framelets

Summary

- Present two types of overcomplete DWT.
- To evaluate the 2X/3X overcomplete DWT I have used it for signal/image denoising and image fusion, and then compared it with the critically-sampled DWT.
- The 2X/3X overcomplete DWT is nearly shift-invariant and avoids some of the artifacts that arise when the critically-sampled DWT is used for signal/image denoising and image fusion.
- The 2X/3X overcomplete DWT both provide significant performance gains in signal/image denoising and image fusion.

For Reading

A. Ron. and Z. Shen.
Affine systems in $L^2(\mathbb{R}^d)$:The analysis of the analysis operator.
Journal of functional analysis, 148:408–447, 1997.

I. W. Selesnick and A.F. Abdelnour.
Symmetric wavelet tight frames with two generators.
Applied Computational Harmonic Analysis, 17:211–225, 2004.

I. W. Selesnick.
A Higher-Density Discrete Wavelet Transform.
IEEE Transactions on Signal Processing, Preprint.

For Reading

A. Ron. and Z. Shen.
Affine systems in $L^2(\mathbb{R}^d)$:The analysis of the analysis operator.
Journal of functional analysis, 148:408–447, 1997.

I. W. Selesnick and A.F. Abdelnour.
Symmetric wavelet tight frames with two generators.
Applied Computational Harmonic Analysis, 17:211–225, 2004.

I. W. Selesnick.
A Higher-Density Discrete Wavelet Transform.
IEEE Transactions on Signal Processing, Preprint.

For Reading

- A. Ron. and Z. Shen.
  Affine systems in $L^2(\mathbb{R}^d)$:The analysis of the analysis operator.
  Journal of functional analysis, 148:408–447, 1997.
- I. W. Selesnick and A.F. Abdelnour.
  Symmetric wavelet tight frames with two generators.
  Applied Computational Harmonic Analysis, 17:211–225, 2004.
- I. W. Selesnick.
  A Higher-Density Discrete Wavelet Transform.
  IEEE Transactions on Signal Processing, Preprint.

For Further Reading

M. Choi, R.Y. Kim, M.R. Nam, and H.O. Kim.
Fusion of Multispectral and Panchromatic Satellite Images Using the Curvelet Transform.
IEEE Geoscience and Remote Sensing letters,2:136–140, 2005.

M. Choi.
A New Intensity-Hue-Saturation Fusion Approach to Image Fusion with a Tradeoff Parameter.
IEEE Transactions on Geoscience and Remote Sensing, Vol.44, No.6, JUNE 2006.

For Further Reading

- M. Choi, R.Y. Kim, M.R. Nam, and H.O. Kim.
  Fusion of Multispectral and Panchromatic Satellite Images Using the Curvelet Transform.
  IEEE Geoscience and Remote Sensing letters,2:136–140, 2005.
- M. Choi.
  A New Intensity-Hue-Saturation Fusion Approach to Image Fusion with a Tradeoff Parameter.
  IEEE Transactions on Geoscience and Remote Sensing, Vol.44, No.6, JUNE 2006.

For Further Reading

M. Choi.
Introduction of a Symmetric Tight Wavelet Frame to Image Fusion Methods Based on Additive Wavelet Decomposition.
IEEE Transactions on Geoscience and Remote Sensing, Preprint.